

# Mapping a Functional Viral Protein in Solution Using Synchrotron X-ray Footprinting Technology

SAYAN GUPTA,<sup>1</sup> WALTER F. MANGEL,<sup>2</sup> MICHAEL SULLIVAN,<sup>1</sup> KEIJI TAKAMOTO,<sup>1</sup> AND MARK R. CHANCE<sup>1</sup>

<sup>1</sup>Center for Synchrotron Biosciences and Department of Biophysics and Physiology, Albert Einstein College of Medicine, Bronx, NY 10460, USA

<sup>2</sup>Department of Biology, Brookhaven National Laboratory, Upton, NY 11973-5000, USA

Understanding the atomic details of biomolecular structure and dynamics in solution is essential to provide molecular descriptions of biological function inside living cells. In studying structure and dynamics at atomic resolution, both Nuclear Magnetic Resonance (NMR) and X-ray crystallography are important tools. Both techniques have a common limitation in that they need a high concentration of the biomolecule in solution or for crystal formation. Synchrotron footprinting (SF) is used for the examination of folding and other conformational changes and identification of binding interactions with high resolution. Previously we had reported on the use of the technique to probe nucleic acid structure and dynamics [1]. In the present report we illustrate the use of SF to analyze protein structure in solution with side chain level resolution using picomoles of material.

SF has been successfully used to analyze the structure of proteins under a number of solution conditions and in various complexes with other proteins and nucleic acids [2–8]. Synchrotron X-rays generate hydroxyl radicals from water that modify solvent accessible and reactive side-chains of proteins [1–4,6]. Due to the stable nature of the radiolyzed products the extent of these reactions are further investigated using mass spectroscopy for proteins [3,4] and gel electrophoresis for nucleic acids [2,9]. Since the radiolysis timescale is short using synchrotron light, secondary radiolysis effects are minimal and time-resolved studies can be accomplished as well. In this report we will discuss how SF is applied to study the structure and function of the human adenovirus serotype 2 proteinase (AVP), which is required for the synthesis of infectious virus [10, 11].

## The adenovirus proteinase

AVP is originally synthesized in the infected host cell as an inactive protein and requires two cofactors for maximal proteinase activity [10,11]. One cofactor is the eleven amino acid residue peptide pVIc, originating from the C-terminus of the precursor protein pVI. This peptide is covalently linked to AVP through a disulfide bond as well as by charge-charge and hydrogen bonding interactions [12,13]. The second cofactor is the viral DNA. The  $K_m$  (apparent affinity constant) for proteinase activity is reduced 10-fold upon binding each cofactor sepa-

ately. However, a cooperative effect is observed in the presence of both cofactors, resulting in an overall 34,000-fold increase in the macroscopic kinetic constant ( $k_{cat}/K_m$ ) compared to free AVP (Figure 1a) [14]. The location of the pVIc binding site on AVP is known from the crystal structure (Figure 1b) [12,13] but the mode of DNA binding is unknown. The structure of AVP has two major domains (D1 and D2) with the active site sandwiched between the domains. Active site residues His-54, Glu-71 and Cys-122, which are located deep within this cleft, are entirely conserved.

## Synchrotron protein footprinting

### At the beamline

SF is carried out at the X28C beamline of the National Synchrotron Light Source (NSLS) at Brookhaven National Laboratory (BNL). The beamline provides white synchrotron light with an effective energy range of 6–20 keV [15]. Figure 2 illustrates the experimental set-up for footprinting studies. Approximately 6 milliradians of unfocused beam exits the beam pipe through a beryllium window (at vacuum). The beam then falls on either an electronic shutter (Vincent Associates, Rochester, NY) on a stand for equilibrium or slow time resolved experiments, or on the flow cell of the stopped-flow (KinTek Corp., Austin, TX) device for fast time-resolved experiments. Both the stand and the Kintek set-up are mounted on a precision motorized table to permit vertical beam alignment. The electronic shutter is used to control time of exposure on the sample placed inside a microfuge (5  $\mu$ l volume) within the sample holder (see Figure 2). The trigger for the electronic shutter is given from outside the hutch after opening the interlocked beamline shutter. The electronic shutter is equipped with a 1-mm platinum/iridium alloy plate capable of blocking X-rays up to energy of 30 keV and can reliably operate with exposures as short as 7 msec. Prior to the experiment, the beam is aligned with a photodiode mounted mechanically just behind the sample holder so that the most intense beam falls symmetrically on the 2 mm diameter area of the 5  $\mu$ l sample meniscus inside the microfuge tube. The temperature of the sample holder can be thermostatically controlled. For fast time-resolved experiments, the customized KinTek

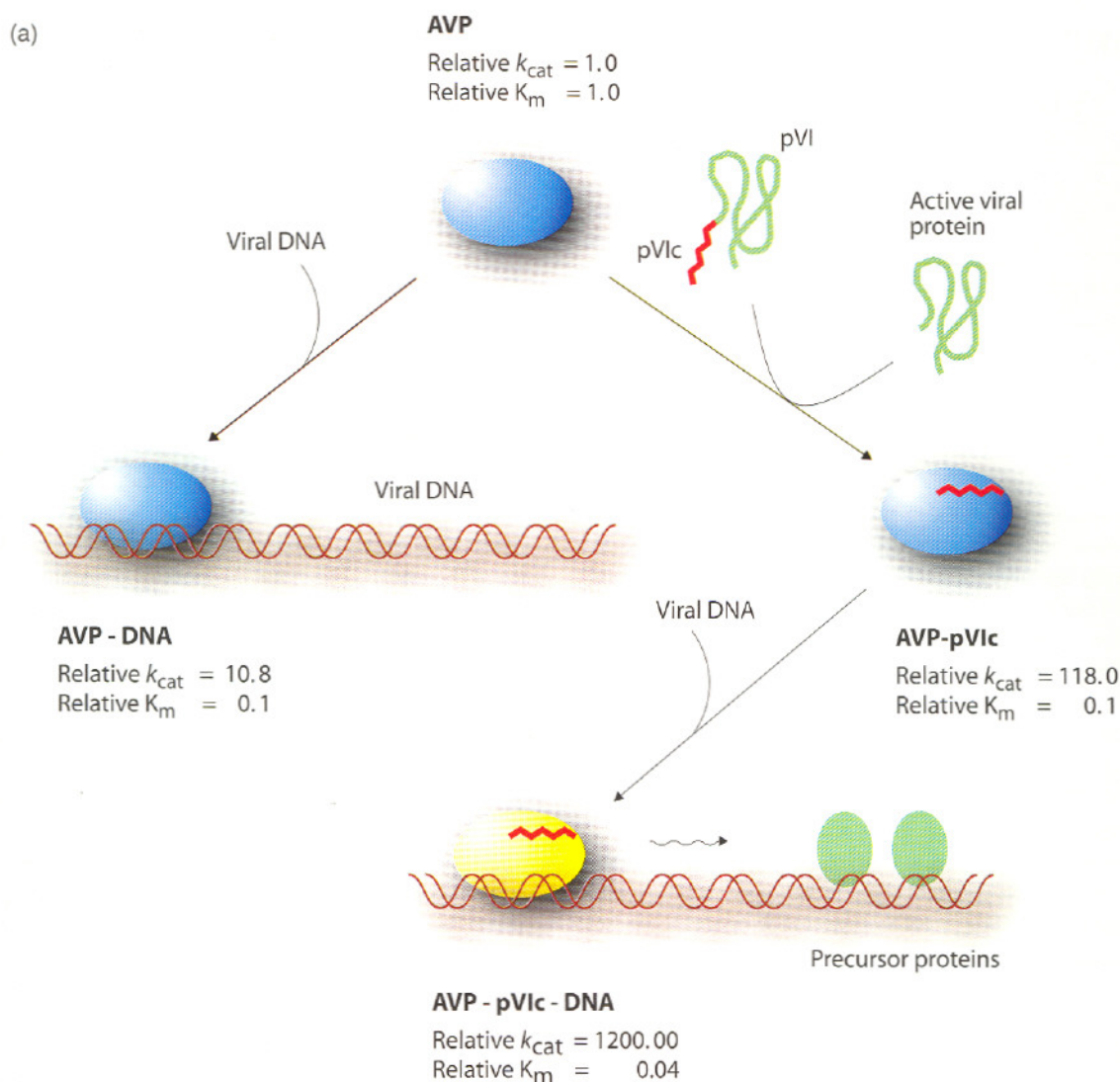


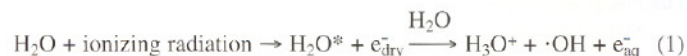
Figure 1 (a): A model for temporal and spatial control of enzymatic activity by cofactors. AVP activity is increased by both peptide and DNA binding. The full activated complex can move along the DNA via one-dimensional diffusion, cleaving virion precursor proteins.

quench-flow apparatus is used to rapidly mix two solutions in a T-mixer in advance of exposure to the X-ray beam. After the required delay, the mixed solution is passed through an exposure cell. Exposures are controlled by adjusting the speed of the flow, which in turn is controlled by the KinTek syringe drive motor system.

#### Theory of radiolysis

In the energy range of the photons of the synchrotron beam at the X28C beamline of NSLS, the interaction of X-rays and water involves both the photoelectric effect and Compton scattering [9,15]. Such photons have sufficient energy to eject an electron from water. The ionized

water molecule reacts with other water molecules to yield hydroxyl radicals according to the following reaction scheme:



Due to the high repetition rate of the NSLS X-ray Ring (ring frequency = 52 MHz), a steady state hydroxyl radical concentration is maintained during the millisecond X-ray beam exposure of the sample. Moreover, since the sample concentrations are extremely low compared to the concentration of bulk phase water, direct interactions between X-rays and macromolecules are minimal in typical footprinting experiments. Thus,

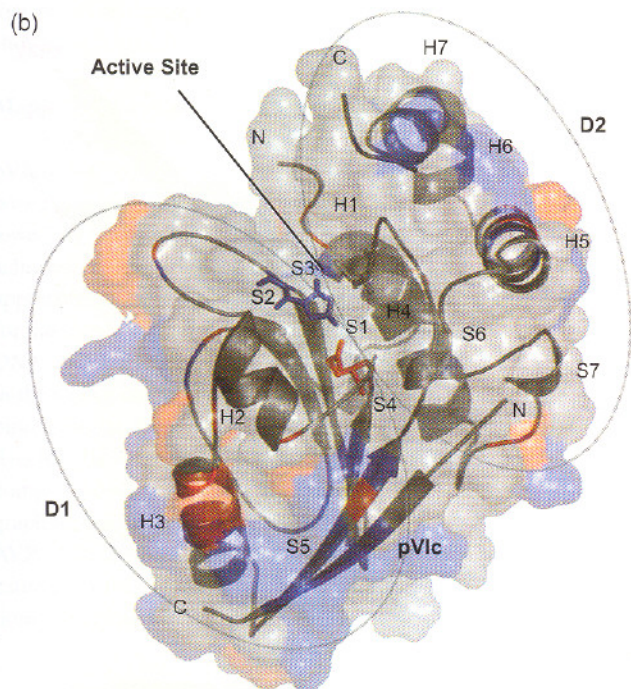


Figure 1(b): Ribbon representation of the AVP-pVlc complex. The protein consists of two domains, D1 and D2. D1 consists of sheets S1-S4 and helices H2 and H3 from the N-terminal half. D2 is composed of helices H4 to H7 and sheets S6 and S7 from the C terminal half of the protein, as well as H1, which is from N-terminus. The outer surface area of the AVP-pVlc complex is shown in transparent color. The distribution of the basic (blue) and the acidic (red) amino acid residues are shown.

the indirect solution chemistry of the hydrated electrons and hydroxyl radicals govern the chemical oxidations observed.

#### Chemistry of protein footprinting

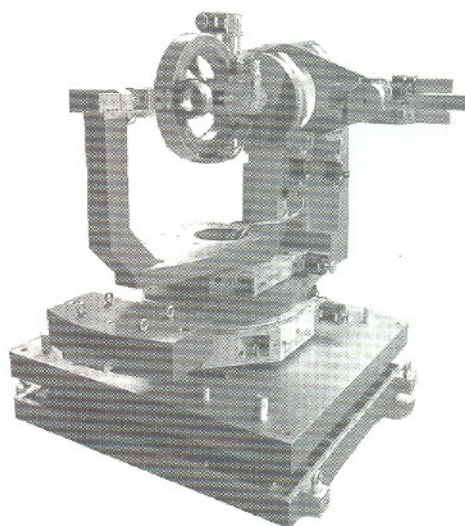
For proteins, chemical modification of the amino acid side chains, backbone cleavage and cross-linking all can occur as a function of radiolysis [4]. Synchrotron radiolysis of the model peptides and proteins have revealed that amino acid side chain oxidations are dominant; reactions leading to backbone cleavage are much slower and cross-linking is minimal due to the low concentrations of macromolecules [3,4,15]. Mass spectrometry is ideally suited to detect the signature mass changes as a function of specific side chain oxidation [3, 4]. Aliphatic and aromatic amino acids suffer mass additions of +16 or +14 Da as a result of alcohol and ketone formation [16,17]. The amino acid histidine experiences ring opening; the observed products have mass shifts of -22, -23, -10 and +5 Da. The amino acid arginine experiences deguanidation with a mass shift of -43 Da [16] while the acidic amino acids glutamate and aspartate undergo oxidative decarboxylation leading to a mass shift of -30 Da [17]. Oxidative decarboxylation is also common at the C-terminal residue [17]. The reactivity of an individual side chain in a pro-



BLAKE INDUSTRIES, INC.

Your complete source for:

Goniometer Heads  
Huber Components  
Complete Diffractometers  
Custom Designs



6+2 - Circle PSI - Diffractometer

More than 4500 professionals at over 1400 research locations have chosen Blake Industries for their X-ray diffraction instrumentation.

Let us put our experience to work for you.

#### BLAKE INDUSTRIES, INC.

660 Jerusalem Road  
Scotch Plains, New Jersey 07076 USA

Tel: +1 908 233 7240

Fax: +1 908 233 1354

E-mail: [blake4xray@worldnet.att.net](mailto:blake4xray@worldnet.att.net)

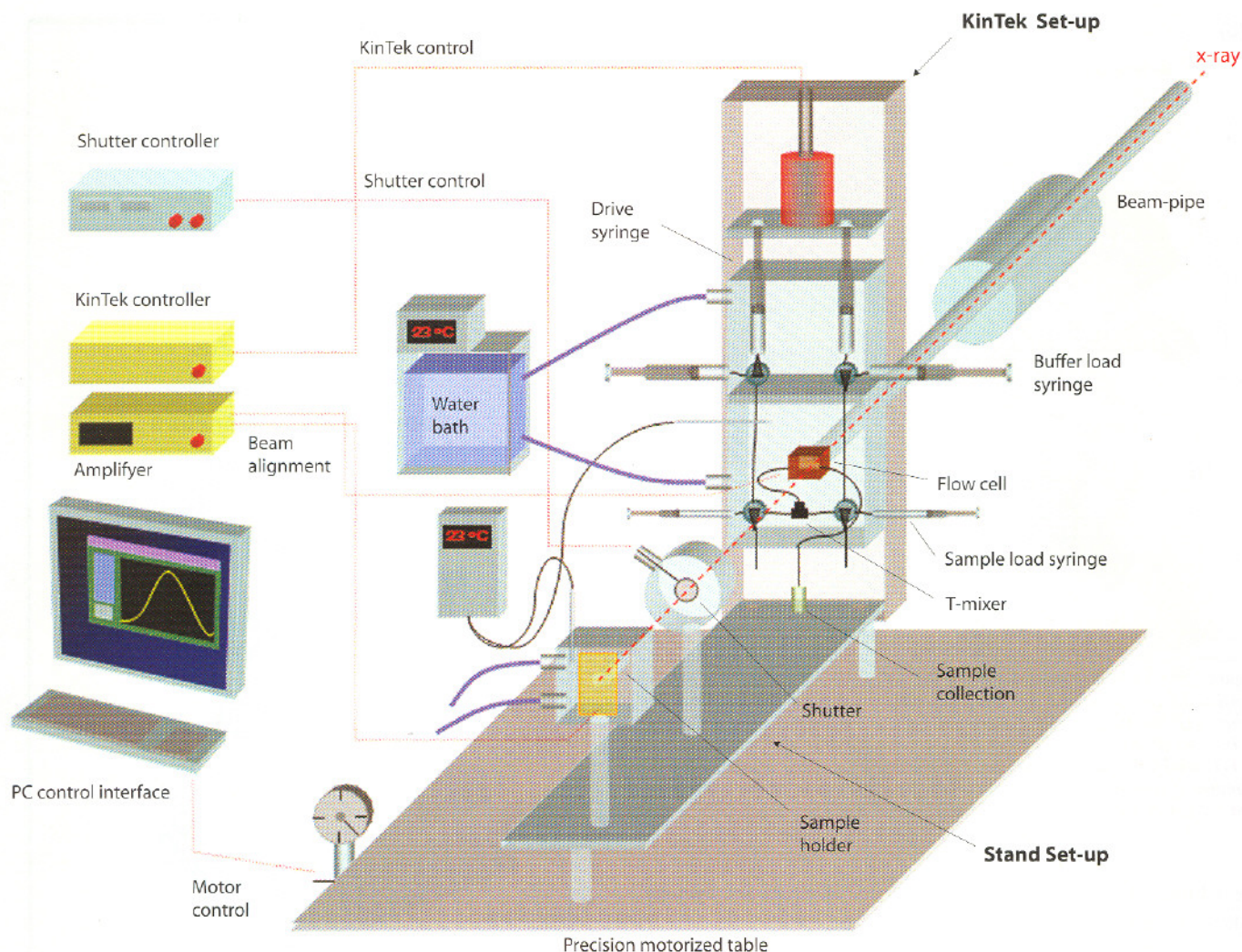


Figure 2: Schematic representation of the experimental setup within the beamline X28C hutch used to conduct synchrotron X-ray footprinting experiments. The PC interface for the beam alignment, KinTek controller, and the shutter controller are situated outside the X28C hutch.

tein is governed by this intrinsic reactivity attenuated by solvent accessibility within the protein structure [4].

*The technique*

For protein footprinting studies,  $\mu\text{M}$  concentrations of the protein in different functional states are irradiated for different exposure times ranging from 10–300 msec. For each exposure time the radiolytically modified protein is then digested using specific proteolytic enzymes to provide regions of interest for structural analysis. The unmodified and modified peptide fragments are isolated and detected in liquid chromatography coupled electrospray mass spectrometry (LC-ESI-MS) followed by fragmentation using tandem mass spectrometry to determine

the specific oxidation sites that are the experimental probes of structure [3,4]. The fraction modified for peptide fragments at each exposure time is calculated from the peak intensities in the electrospray mass spectrometry (ESI-MS) or in matrix-assisted laser desorption/ionization mass spectrometry (MALDI-MS) [3,4] and plots of the fraction of unmodified peptide fragments versus exposure time (dose response plot) are compared for different experimental conditions. Sites of protection (within a macromolecular interface) will show reductions in oxidation rate as a function of complex formation. However, footprinting, as a local probe, only shows the response of a specific site to changes in ligation; thus a specific probe site can show increases, decreases, or no change in reactivity as a function of ligand binding. These data must

then be interpreted in the context of available structural data. Figure 3 shows the schematics of the protein footprinting assay.

#### Mapping the cofactors binding to AVP

AVP and its binary (AVP-DNA and AVP-pVIC) and ternary (AVP-pVIC-DNA) complexes all at  $\mu\text{M}$  concentrations in solution were exposed to white synchrotron X-ray radiation for periods of 0–150 ms followed by digestion with proteases. Separation of the fragments was achieved by reverse phase liquid chromatography, and MS and MS/MS approaches were used as described above [6]. The dose-response curves for the tryptic and chymotryptic peptides obtained from free AVP, AVP-DNA, AVP-pVIC and AVP-pVIC-DNA demonstrated significant changes in the rate of modification (both increases and decreases) upon cofactor binding to the AVP molecule for many peptides. The modification rate data for all nine tryptic peptides of AVP and the AVP-pVIC-DNA ternary complex as well as that for six chymotryptic peptides are shown in bar graph format in Figure 4a. The result is also schematically shown on the AVP-pVIC complex (Figure 4b), indicating the locations of the modifications. In the figure the peptides exhibiting DNA dependent protections are colored in red, while the pVIC dependent protections are col-

ored pink. Peptides exhibiting DNA or pVIC dependent enhancements in reactivity are colored in blue. Figure 4b also illustrates the amino acid side chain residues or SF probes undergoing modification as detected by MS/MS analysis. The results suggest sites of interaction (represented as protections) between cofactors pVIC and DNA with AVP as well as the allosteric effects of the cofactor binding in the active site cleft distal to the cofactor binding sites.

#### pVIC binding to AVP

The interactions of AVP and pVIC are well understood from the 1.6 Å resolution crystal structure of AVP-pVIC complex and include hydrogen bonds, ion pair interactions, van der Waals interactions, and a disulfide bond [12,13]. The solution footprinting data is entirely consistent with these crystallographic predictions, as peptide 104–109 (which contains Cys-104 and Leu-107 as probe sites) experiences a four-fold decrease in reactivity upon pVIC binding to AVP, consistent with the significant reductions in solvent accessibility predicted from the crystallographic data [6]. Within peptide 142–147, the highly conserved Met-147 in domain D2 forms an inter-domain hydrogen bond with the entirely conserved Gly-1' at the N terminus of pVIC. This peptide also



## «Easy close» All-metal Angle Valves

Series 54 for UHV applications



- High conductance
- No torque wrench needed
- Maintenance-free
- Low price

**Now available**  
DN 16 to 63

<b>Swiss Headquarters</b> Tel ++41 81 771 61 61 reception@vat.ch	<b>VAT Japan</b> Tel (045) 333 11 44 sales@vatskk.co.jp	<b>VAT Taiwan</b> Tel 03 516 90 88 taiwan@vatvalve.com	<b>VAT France</b> Tel 01 69 20 69 11 france@vatvalve.com	<b>VAT U.K.</b> Tel 01926 452 753 uk@vatvalve.com
<b>VAT USA</b> Tel (781) 935 1446 usa@vatvalve.com	<b>VAT Korea</b> Tel 031 704 88 57 korea@vatvalve.com	<b>VAT Benelux</b> Tel ++31 (30) 6018251 benelux@vatvalve.com	<b>VAT Germany</b> Tel (089) 46 50 15 deutschland@vatvalve.com	<b>www.vatvalve.com</b>



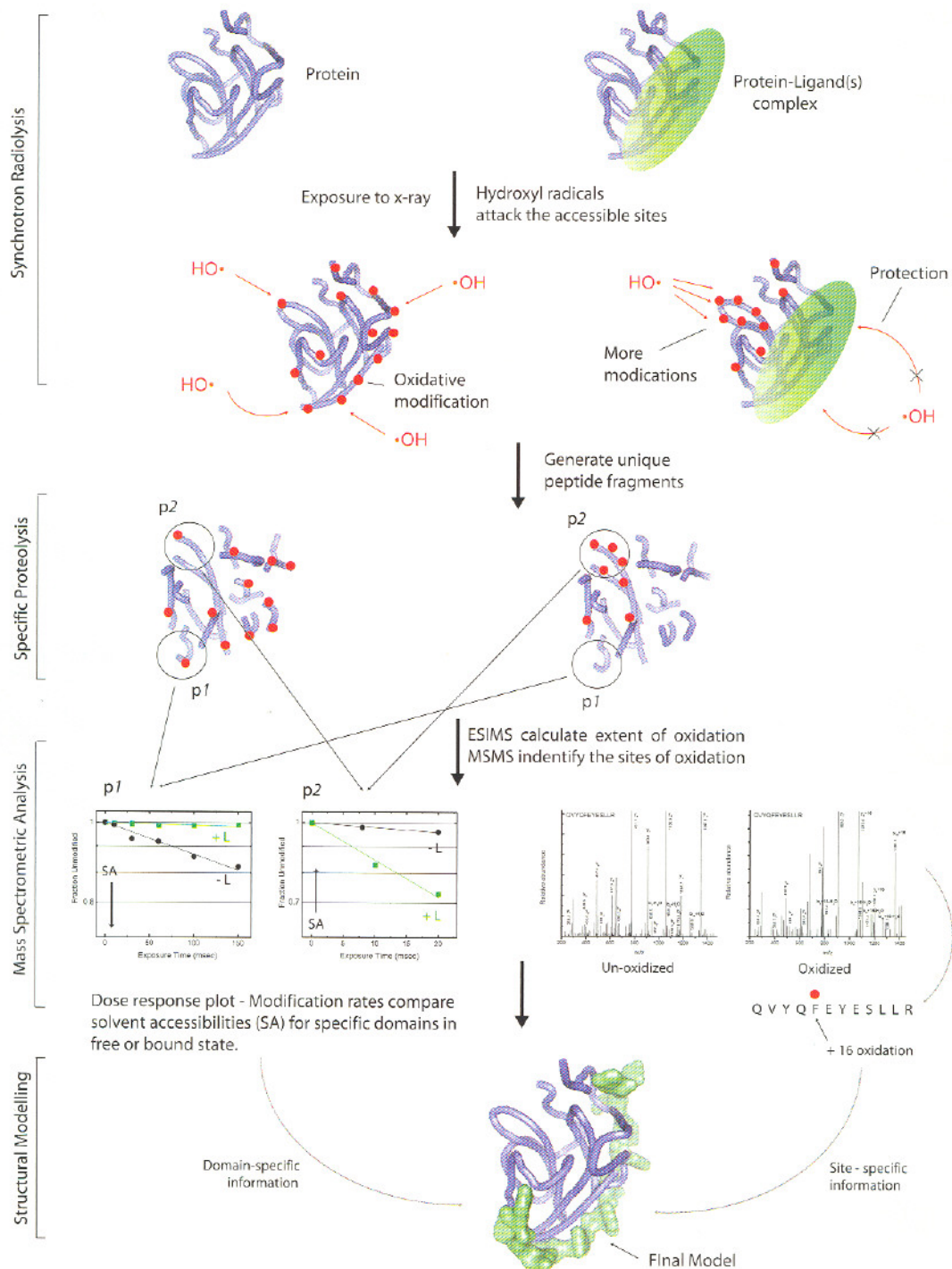


Figure 3: Schematic representation of protein footprinting using synchrotron radiolysis and mass spectroscopy. The examples emphasize the protection formed in the interface of a protein-ligand complex as well as allosteric conformation changes that can result in increases in reactivity upon ligand binding; however, the comparison could be for any two or multiple functional states of the protein of interest.

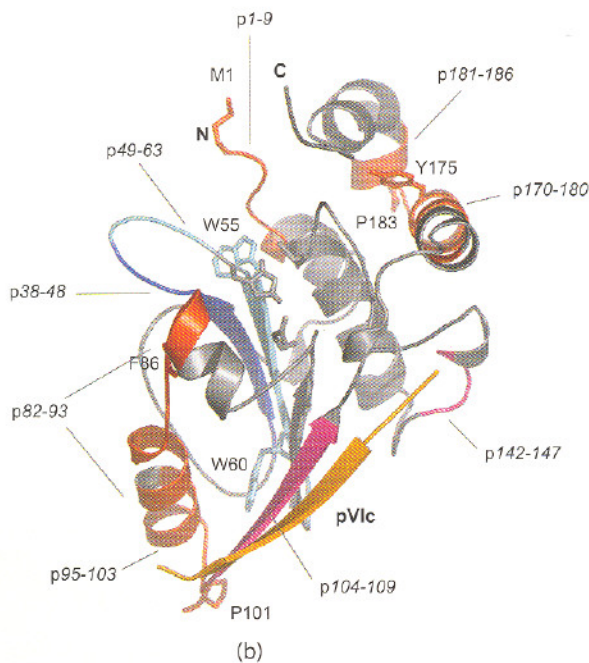
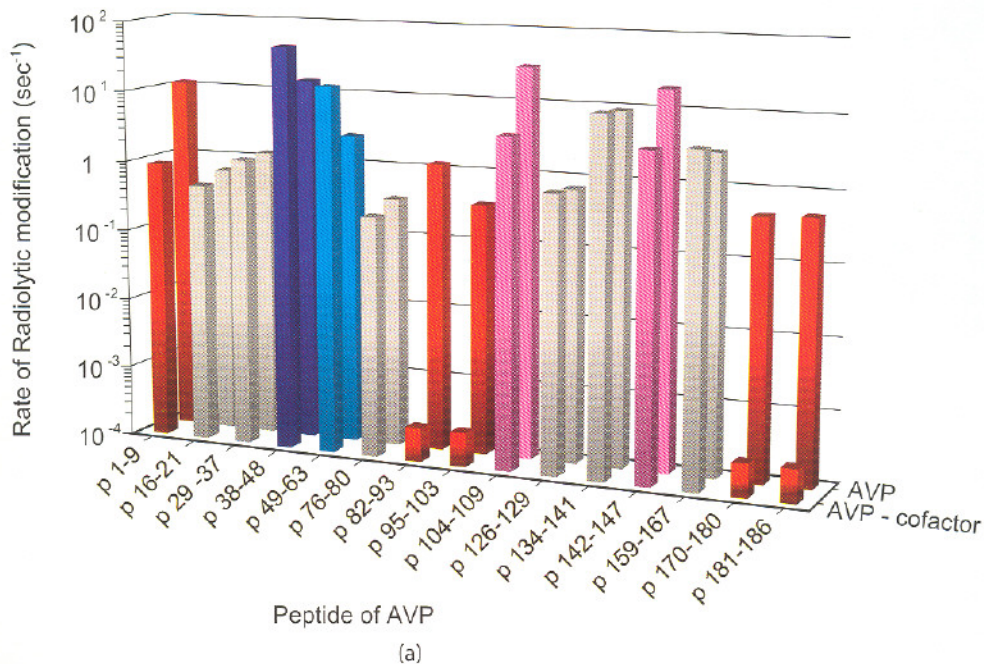
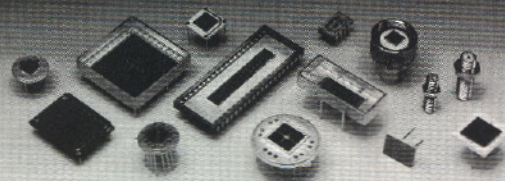


Figure 4: (a) Bar graph showing the rate of modification of the tryptic and chymotryptic peptides obtained from free AVP (back row) and of AVP-pVlc-DNA (front row). Since data for the ternary complex of peptides 104–109 and 142–147 were not available, data for the AVP-pVlc complex is shown instead for these peptides. Red in the figure indicates a DNA dependent protection; blue indicates enhancement of reactivity due to cofactor binding; pink indicates pVlc dependent protections; and gray indicates no observed change in reactivity. The identical color scheme is used in Figure 4(b). (b) Ribbon diagram representation of the AVP-pVlc complex, pVlc is shown in orange. The peptides that showed a decrease in modification rate due to DNA (or pVlc) binding are shown in red (pink). The peptides that showed an increase in modification rate due to cofactor binding are shown in blue. The side chain probe residues identified by MS/MS are indicated.

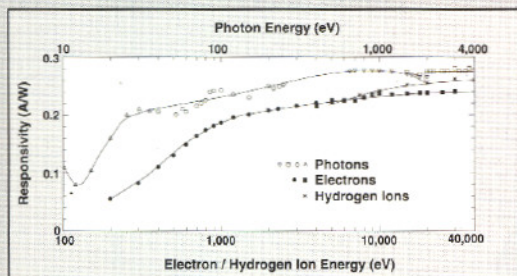
# ABSOLUTE

XUV SILICON PHOTODIODES

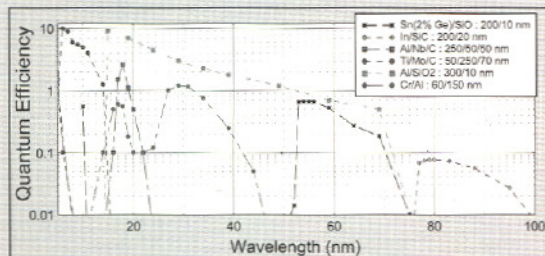


## Features

- 100% Internal Carrier Collection Efficiency
- 8 Decades of Linearity
- No Change in QE with 100 Mrad (Si) 124 eV Photons
- May be Operated Without Bias
- Cryogenically and UHV Compatible



TYPICAL RESPONSIVITY OF AXUV PHOTODIODES TO PHOTONS, ELECTRONS AND HYDROGEN IONS



REPRESENTATIVE AXUV PHOTODIODES WITH INTEGRATED FILTERS



INTERNATIONAL RADIATION DETECTORS INC.

2527 West 237th Street, Unit C • Torrance, California 90505-5243  
(310) 534-3661 • FAX (310) 534-3665 • email: irdinc@earthlink.net

<http://www.ird-inc.com>

DEVELOPED IN COLLABORATION WITH NIST, NOAA, NIH, LLNL, LANL, NCAR

experiences a protection in the AVP-pVlc binary complex consistent with this interaction [6].

### Cofactor induced conformational changes

Increased rates of modification for peptides 38–48 and 49–63 upon cofactor binding indicated increased “spatial” availability of the active site cleft to substrates as well as changes in the chemical reactivity of residues within the cleft (Figures 4a,b). The reactivity of peptide 38–48 was not influenced by DNA binding alone but exhibited a 2-fold increased reactivity upon binding pVlc [6]. Unlike peptide 38–48, the reactivity of peptide 49–63 is increased upon either DNA binding (2-fold) or pVlc binding alone (6-fold) [6]. For free AVP, Trp-60 was the sole probe residue while in the ternary complex, Trp-55 and Met-66, which are within 5 Å of the active site His-54 and Cys-122 residues, became more solvent accessible and were oxidized [6]. Trp-60 and Trp-55 are conserved, primarily to preserve the architecture of the binding pocket. These data provide convincing evidence that cofactor binding to AVP changed the structure at the active site. In the case of pVlc binding, a possible molecular explanation for this reactivity change includes subdomain rearrangements mediated by interactions of the pVlc peptide across the interface between domains 1 and 2 (Figure 1b) [6]. This raises the question as to the molecular mechanisms by which DNA binding provides a similar activation, as well as how the two cofactors work together to provide maximal activity for the enzyme.

### Binding of DNA to AVP

Biochemical studies show that DNA binding is not sequence specific [10] and both electrostatic and non-electrostatic forces are important for the binding interactions [14]. Figure 1b depicts the surface charge distribution on AVP; positively charged clusters are seen that may be involved in nonspecific DNA binding [13]. Footprinting data clearly indicate DNA dependent protections for five peptides (Figure 4a,b) where the extent of protection (>90%) was consistent with burial of the respective probe sites in a macromolecular interface [18–20]. The site-specific protections were adjacent to the positively charged surface patches on the AVP. The buried probe residues are indicated in Figure 4b and include Met-1, Pro-183 and Tyr-175 in D2, which are located on the opposite side of the molecule to Phe-86 and Pro-101 in D1. Since the stoichiometry of DNA-AVP binding is 1:1 for the 12-mer ssDNA used here [14], we considered the possibility that the DNA could be stretched across the AVP molecule so as to bury residues within both D1 and D2.

### Detailed model of DNA-AVP interactions

The DNA-AVP interface was modeled using a 12-mer single stranded DNA with the sequence GACGACTAGGAT. The constraints in the modeling included: DNA dependent protection of the above probe residues; satisfaction of potential favorable charge or base stacking interactions; use of conserved residues to provide the trace of the DNA-

AVP interaction; and reasonable constraints on the bond lengths and angles of the macromolecules. The final model (Figure 5) satisfies many of these constraints, in particular solvent accessibility calculations; the coordinates of the ternary complex compared to that of the AVP-pVlc binary complex showed DNA-dependent protections from solvent for Phe-86, Pro-101, Pro-183, and Tyr-175.

Although this model of DNA binding was constructed based on predicted interactions with a 12-mer ssDNA, we suggest that it provides a general model of AVP-DNA binding. AVP binds longer single stranded sequences than a 12-mer and, *in vivo*, binds to double stranded DNA. The model predicts a significant bending of the single stranded DNA, which is obviously quite flexible. However, bending of double stranded DNA in the process of protein binding is well preceded [21–24]. Thus, the combination of conserved positively charged patches on AVP and its conserved aromatic residues that are poised for base stacking interactions provides a facile surface for binding and bending double stranded DNA. Thus, our model provides an overall framework

for predicting AVP-DNA interactions and suggests that DNA binding provides a molecular strap re-orienting the positions of the two subdomains directly influencing the reactivity of the active site. In addition, both pVlc and DNA may independently provide this re-orientation as well as drive it cooperatively to fully activate AVP.

#### Concluding remarks

Radiolytic protein footprinting coupled to mass spectrometry has been developed over the last several years into a viable approach for analyzing protein structure and dynamics. In this account we report the application of synchrotron protein footprinting to determine the structural changes within AVP upon formation of complexes with its activating cofactors. The data revealed cofactor dependent conformational changes at the catalytic site related to functional activation. Footprinting data of the binary complex of AVP with DNA as well as the ternary complex of AVP and both its cofactors revealed potential sites of DNA contact with AVP. A molecular model of the AVP-DNA-pVlc ternary complex is

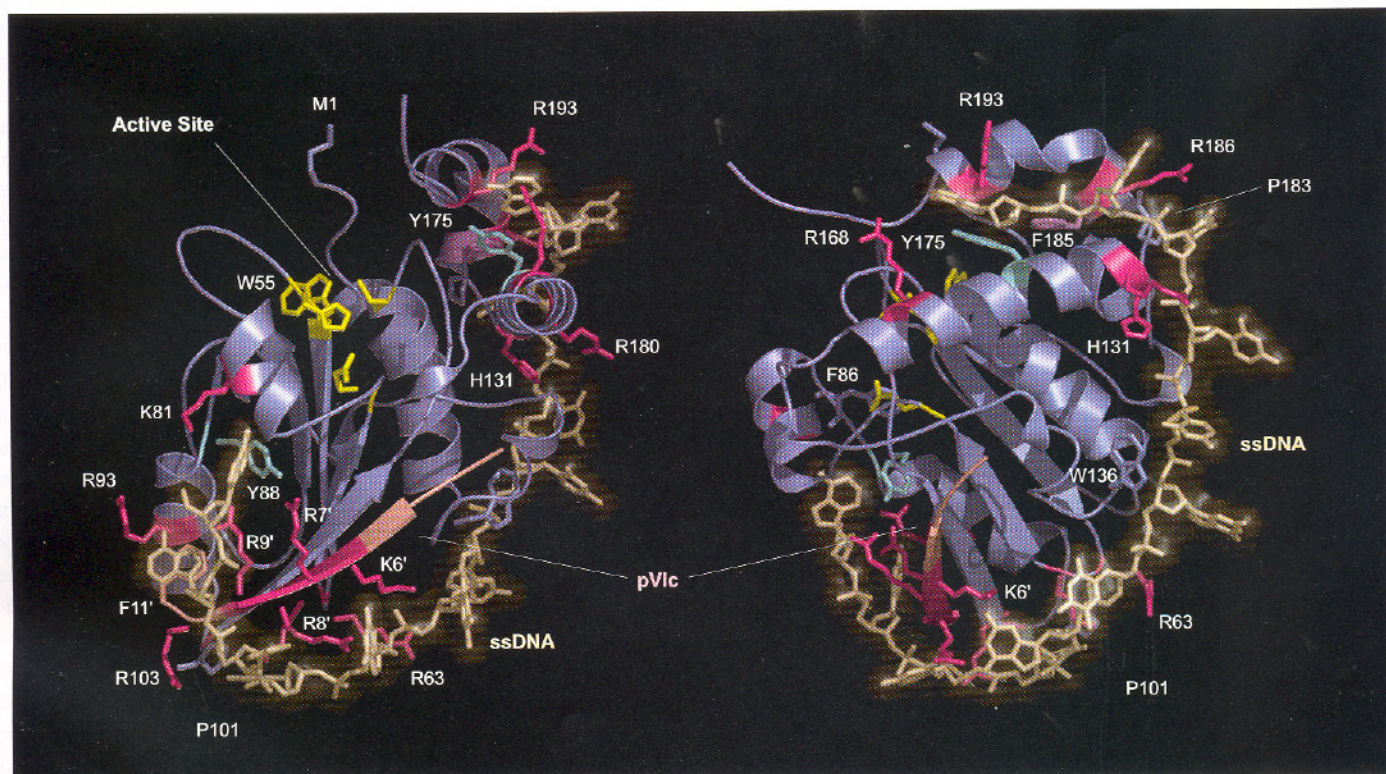


Figure 5: A model for DNA binding to AVP-pVlc complex is shown in two different orientations. The AVP-pVlc complex is shown in ribbon format, where AVP and pVlc are colored in slate and light pink, respectively. The ssDNA has a stick representation and is colored off-white. The amino acid residues proposed to interact with DNA are represented with dark pink for basic (Arg, His and Lys), cyan for Tyr, magenta for Phe from AVP and light pink for Phe from pVlc. The probe residues identified by MS/MS are also indicated and highlighted with the same colors of the AVP ribbon diagram. The active site residues and Trp-55 are also colored yellow.

proposed that is consistent with the footprinting data and the observed sequence conservation, as well as providing a molecular mechanism of activation that explains the synergistic effects of the two cofactors. ■

### Acknowledgements

This research is supported in part by The Biomedical Technology Centers Program of the National Institute for Biomedical Imaging and Bioengineering (P41-EB-01979, M.R.C.), the Innovative Molecular Analysis Technologies Program of the National Cancer Institute (R33-CA-83179, M.R.C.), the Office of Biological and Environmental Research of the U.S. Department of Energy under Prime Contract DE-AC0298CH10886 with Brookhaven National Laboratory (W.F.M.), and by National Institutes of Health Grant AI41599 (W.F.M.). The National Synchrotron Light Source is supported by the Department of Energy, Office of Science.

### References

- Chance, M. R., Brenowitz, M., Sullivan, M., Selavi, B., Maleknia, S., Ralston, C. "A New Method for Examining the Dynamics of Macromolecules: Time-Resolved Synchrotron X-ray "Footprinting," *Synchrotron Radiation News* **11**, 7-16 (1998).
- Takamoto, K. G., Chance, M. R. "Footprinting Methods to Examine the Structure and Dynamics of Nucleic Acids," *Encyclopedia of Molecular Cell Biology and Molecular Medicine*, 2nd Ed., R. Meyers, Editor, Wiley Inc., 521-548 (2004).
- Guan, J.-Q., Chance, M. R. "Footprinting Methods to Examine the Structure and Dynamics of Proteins," *Encyclopedia of Molecular Cell Biology and Molecular Medicine*, 2nd Ed., R. Meyers, Editor, Wiley Inc., 549-568 (2004).
- Kiselar, J. G., Maleknia, S. D., Sullivan, M., Downard, K. M., Chance, M. R. "Hydroxyl radical probe of protein surfaces using synchrotron X-ray radiolysis and mass spectrometry," *Int J Radiat Biol* **78**, 101-114 (2002).
- Guan, J. G., Almo, S. C., Chance, M. R. "Synchrotron Radiolysis and Mass Spectrometry: A New Approach to Research on the Actin Cytoskeleton," *Acc. Chem. Res.* **37**, 221-229 (2004).
- Gupta, S., Mangel, W. F., Baniecki, M. L., McGrath, W. J., Takamoto, K. G., Chance, M. R. "DNA Binding Provides a Molecular Strap Activating the Adenovirus Proteinase," *Mol. & Cell Proteomics* **3**, 950-959 (2004).
- Kiselar, J. G., Janmey, P. A., Almo, S. C., Chance, M. R. "Visualizing the Ca<sup>2+</sup> Dependent Activation of Gelsolin by Using Synchrotron Footprinting," *Proc. Nat. Acad. Sci.* **100**, 3942-3947 (2003).
- Liu, R., Guan, J. Q., Zak, O., Aisen, P., Chance, M. R. "Structural Reorganization of Transferrin C-Lobe and Transferrin Receptor Upon Complex Formation: C-Lobe Binds to the Receptor Helical Domain," *Biochemistry* **42**, 12447-12454 (2003).
- Ralston, C. Y., Scalvi, B., Sullivan, M., Deras, M. L., Woodson, S. A., Chance, M. R., Brenowitz, M. "Time-resolved synchrotron X-ray footprinting and its application to RNA folding," *Methods Enzymol* **317**, 353-68 (2000).
- Mangel, W. F., McGrath, W. J., Toledo, D. L., Anderson, C. W. "Viral DNA and a viral peptide can act as cofactors of adenovirus virion proteinase activity," *Nature* **361**, 274-275 (1993).
- Baniecki, M. L., McGrath, W. J., McWhirter, S. M., Li, C., Toledo, D. L., Pellicena, P., Barnard, D. L., Thorn, K. S., Mangel, W. F. "Interaction of the human adenovirus proteinase with its 11-amino acid cofactor pVIc," *Biochemistry* **40**, 12349-12356 (2001).
- McGrath, W. J., Ding, J., Didwania, A., Sweet, R. M., Mangel, W. F. "Crystallographic structure at 1.6-Å resolution of the human adenovirus proteinase in a covalent complex with its 11-amino-acid peptide cofactor: insights on a new fold," *Biochim. Biophys. Acta* **1648**, 1-11 (2003).
- Ding, J., McGrath, W. J., Sweet, R. M., Mangel, W. F. "Crystal structure of the human adenovirus proteinase with its 11 amino acid cofactor," *Embo J.* **15**, 1778-1783, (1996).
- McGrath, W. J., Baniecki, M. L., Li, C., McWhirter, S. M., Brown, M. T., Toledo, D. L., Mangel, W. F. "Human adenovirus proteinase: DNA binding and stimulation of proteinase activity by DNA," *Biochemistry* **40**, 13237-13245 (2001).
- Maleknia, S. D., Ralston, C. Y., Brenowitz, M. D., Downard, K. M., Chance, M. R. "Determination of macromolecular folding and structure by synchrotron X-ray radiolysis techniques," *Anal. Biochem.* **289**, 103-115 (2001).
- Xu, G., Takamoto, K. G., Chance, M. R. "Radiolytic Modification of Basic Amino Acids: New Probes for Protein Footprinting," *Anal. Chem.* **75**, 6995-7007 (2003).
- Xu, G., Chance, M. R. "Radiolytic Modification of Acidic Amino Acids: New Probes for Protein Footprinting," *Anal. Chem.* **76**, 1213-1221 (2004).
- Guan, J. Q., Vorobiev, S., Almo, S. C., Chance, M. R. "Mapping the G-actin binding surface of cofilin using synchrotron protein footprinting," *Biochemistry* **41**, 5765-5775 (2002).
- Rashidzadeh, H., Kharapuv, S., Chance, M. R., Brenowitz, M. "Solution Structure and Interdomain Interactions of the *Saccharomyces cerevisiae* "TATA Binding Protein" (TBP) Probed by Radiolytic Protein Footprinting," *Biochemistry* **42**, 3655-3665 (2003).
- Liu, R., Guan, J. Q., Zak, O., Aisen, P., Chance, M. R. "Structural reorganization of Transferrin C-lobe and Transferrin Receptor Upon Complex Formation: C-lobe to the Receptor Helical Domain," *Biochemistry* **42**, 12447-12454 (2003).
- Rice, P. A., Yang, S., Mizuuchi, K., Nash, H. A. "Crystal structure of an IHF-DNA complex: a protein-induced DNA U-turn," *Cell* **87**, 1295-1306 (1996).
- Kim, J. L., Nikolov, D. B., Burley, S. K. "Co-crystal structure of TBP recognizing the minor groove of a TATA element," *Nature* **365**, 520-527 (1993).
- Juo, Z. S., Chiu, T. K., Leiberman, P. M., Baikalov, I., Berk, A. J., Dickerson, R. E. How proteins recognize the TATA box. *J. Mol. Biol.* **261**, 239-254, 1996.
- Kim, Y., Geiger, J. H., Hahn, S., Sigler, P. B. Crystal structure of a yeast TBP/TATA-box complex. *Nature* **365**, 512-520 (1993).